



# 1 **Characterizing four decades of accelerated glacial mass loss in** 2 **the West Nyainqentanglha Range of the Tibetan Plateau**

3 Shuhong Wang<sup>1,2,3</sup>, Jintao Liu<sup>1,2\*</sup>, Hamish D. Pritchard<sup>3</sup>, Linghong Ke<sup>2</sup>, Xiao Qiao<sup>1,2</sup>, Jie  
4 Zhang<sup>1,2</sup>, Weihua Xiao<sup>4</sup>, Yuyan Zhou<sup>4</sup>

5 <sup>1</sup>State Key Laboratory of Hydrology-Water Resources and Hydraulic Engineering, Hohai University, Nanjing  
6 210098, People's Republic of China.

7 <sup>2</sup>College of Hydrology and Water Resources, Hohai University, Nanjing 210098, People's Republic of China.

8 <sup>3</sup>British Antarctic Survey, Cambridge, CB3 0ET, UK.

9 <sup>4</sup>State Key Laboratory of Simulation and Regulation of Water Cycle in River Basin, China Institute of Water  
10 Resources and Hydropower Research, Beijing 100038, China.

11 \*Correspondence: jtliu@hhu.edu.cn; Tel.: +86-025-83787803

## 12 **Abstract:**

13 Glacier retreat is altering the water regime of the Tibetan Plateau (TP) as the region's climate changes, but  
14 there remain substantial gaps in our knowledge of recent glacier loss in this region due to the difficulty of making-  
15 direct high-mountain observations and this limits our ability to predict the future of this important water resource.  
16 Here, we assessed 44 years of glacier area and volume changes in the major West Nyainqentanglha Range (WNT)  
17 that supplies meltwater to the densely populated Lhasa River basin and Nam Co, the second largest endorheic  
18 lake on the TP. Between the two periods 1976-2000 and 2000-2020, we found that the glacier areal retreat rate  
19 was more than doubled (from  $-0.54 \pm 0.21 \text{ \% a}^{-1}$  to  $-1.17 \pm 0.30 \text{ \% a}^{-1}$ ) and surface lowering also accelerated ( from  
20  $-0.26 \pm 0.09 \text{ m w.e.a}^{-1}$  to  $-0.37 \pm 0.15 \text{ m w.e.a}^{-1}$ ) with particularly intense melting after 2014. This acceleration is  
21 similar in both timing and magnitude to that observed for Himalayas glaciers farther south. Besides, the areal  
22 retreat rate and mass loss rate of most glaciers in WNT were not synchronized. To understand the sensitivity of  
23 WNT glaciers to climate forcing, we examined the effects of topography, debris-cover, and the presence of  
24 proglacial lakes on our observed changes. We found consistently faster areal retreat but slower thinning rates on  
25 steeper slopes and an inconsistent relationship with aspect. We concluded that our observed spatial and temporal  
26 patterns of glacier change were dominated by observed local variations temperature and precipitation, the melt-  
27 reducing role of supraglacial debris, and the increasing influence of ice-marginal lakes on glacier retreat.

## 28 **1. Introduction**

29 The Tibetan Plateau (TP) known as the "Water Tower of Asia", is the source of several of Asia's major rivers  
30 (Bolch et al., 2010) and glacial melt on the TP plays an important role in water supply for downstream populations,  
31 agriculture and industries along these rivers (Pritchard, 2019; Viviroli et al., 2007). Climate change over recent



32 decades has boosted river discharge by increasing runoff from shrinking glaciers (Lin et al., 2020; Yao et al., 2007;  
33 Zhang et al., 2011), but this boost will eventually decrease as glacier area declines (Zhao et al., 2019). The  
34 sensitivity of ice loss to climate change is variable, however, and often poorly known, being a function of glacier  
35 size, hypsometry, aspect, debris cover, and the presence of proglacial lakes and ice cliffs, for example. Combined  
36 with uncertainties in ice thickness and future climate scenarios, the timing of peak water runoff and the rate of its  
37 subsequent decline remain key unknowns (Maurer et al., 2019; Nie et al., 2021; Su et al., 2016; Zhao et al., 2019).  
38 It is therefore critical to monitor and analyze glacier change to improve our understanding of its climate drivers,  
39 and to assess its impacts on glacier-fed river basins.

40 Compared with the interpolation of sparse in-situ measurements, satellites can observe glacier change over  
41 much larger areas of remote terrain (Wang et al., 2021). In recent years, our understanding of the state of TP  
42 glaciers has been greatly improved by the increasing coverage and accuracy of multi-source remote sensing  
43 observations of glacier area, volume and mass change from KH-9 (Hexagon military satellites), Landsat, ASTER,  
44 ICESat altimetry, and other Digital Elevation Models (DEMs) constructed by geodetic techniques, and from  
45 GRACE gravimetry (Guo et al., 2015; Kääb et al., 2012; Wang et al., 2021; Zhou et al., 2018). Based on the  
46 KH-9 images and SRTM, for example, Zhou et al. (2018) found that from the mid-1970s to 2000 glaciers in the  
47 northwest TP thinned at  $-0.11 \pm 0.13$  m w.e.  $a^{-1}$  to  $0.02 \pm 0.10$  m w.e.  $a^{-1}$  while those in the southeast part thinned  
48 faster at  $-0.30 \pm 0.12$  m w.e.  $a^{-1}$  to  $-0.11 \pm 0.14$  m w.e.  $a^{-1}$ . Brun et al. (2018) employed ASTER DEMs from 2000-  
49 2006 and showed that glacier mass balance in High Mountain Asia varied from  $-0.62 \pm 0.23$  m w.e.  $a^{-1}$  in eastern  
50 Nyainqentanglha to  $+0.14 \pm 0.08$  m w.e.  $a^{-1}$  in the Kunlun Mountains, and averaged  $-0.14 \pm 0.14$  m w.e.  $a^{-1}$  over  
51 the large Inner TP that includes WNT. Maurer et al. (2019) found a doubling of the Himalayan average loss rate  
52 between the periods 1976-2000 ( $-0.22 \pm 0.13$  m w.e.  $a^{-1}$ ) and during 2000-2016 ( $-0.43 \pm 0.14$  m w.e.  $a^{-1}$ ) using  
53 KH-9 and ASTER DEMs. These studies showed that glacier changes on and around the TP have marked spatial  
54 and temporal heterogeneity, likely associated in part with variable glacial sensitivity to climate change (Yao et al.,  
55 2012).

56 The drivers of regional glacier loss include, for example, a jump in mean annual temperature and  
57 precipitation in the Yarlung-Zangpo River basin around 1997 (Wang et al., 2021) and an accelerating warming  
58 trend over the TP between the periods 1980-1997 and 1998-2013 (from  $0.21$  °C to  $0.25$  °C decade $^{-1}$ ) (Duan &  
59 Xiao, 2015). Modulating the effect of these climatic drivers are local factors including glacier topography, debris-  
60 cover and, glacial lakes (Brun et al., 2018, 2019; Ke et al., 2020; Maurer et al., 2019; Pandey et al., 2017; Yao et  
61 al., 2012). Some studies have analyzed the melt-inhibiting effect of debris cover and melt-promoting effect of  
62 proglacial lakes on glacier ablation since 2000 (Ke et al., 2020; Vincent et al., 2016), but with the potential for



63 KH-9 in 1976, SRTM in 2000, ASTER in 2000-2020 and aerial mapping Landsat 1996-2020 through time, we  
64 are now able to assess glacier area and mass change in the WNT in relation to both regional climatic drivers and  
65 local modulating factors.

66 The WNT, in the south-eastern TP (Figure 1), is located in the transition zone between the two large-scale  
67 atmospheric circulation patterns characterized respectively by dominant westerlies and the Indian summer  
68 monsoon. It holds an abundance of glaciers and glacial-fed lakes, notably Nam Co Lake (Figure 1), whose rising  
69 water levels indicate a water imbalance primarily due to recently intensified glacier melting (Bolch et al., 2010),  
70 as supported by mass balance data from Zhadang Glacier and other hydrological observations from 2007 to 2011  
71 (Zhou et al., 2013). The number and area of supraglacial lakes (of  $>0.0036$  km<sup>2</sup>) in the WNT also increased  
72 between 1976 and 2018 by 56% and 35% respectively due to the increase in glacial meltwater (Luo et al., 2020).  
73 In the relatively densely-populated Lhasa Basin to the southeast of WNT, Lin et al. (2020) found that a water  
74 imbalance also existed using the first and second Chinese Glacier Inventory in 1960 and 2009. Despite these  
75 extensive changes and large affected population, logistical constraints have meant that in situ glacier mass balance  
76 records are limited to a few low-lying, small glaciers that are unlikely to be representative of the broader region  
77 (Kääb et al., 2012; Li & Lin, 2017; Yao et al., 2012). Similarly, glacier volumes in the Chinese Glacier Inventory  
78 were primarily calculated indirectly by area-volume scaling, and limited direct observations mean that these  
79 volume have larger uncertainty (Bahr et al., 1997; Bahr et al., 2015). Detailed investigation of the WNT glacier  
80 area change and mass balance on a longer time scale is therefore a high priority.

81 Investigations of WNT glacier area have so far focused on the period before 2014 ( Bolch et al., 2010; Wu  
82 et al., 2016). For glacier mass balance, most studies focus on after 2000 (Li & Lin, 2017; Neckel et al., 2014; Ren  
83 et al., 2020; Zhang & Zhang, 2017). There are limited discussions on local glacier changes in the WNT region  
84 from before 2000, although Zhou et al. (2018) included this area in his study of glacier mass balance on the TP  
85 and its surroundings from the mid-1970s to 2000 and did not present the characteristics of glacier changes in detail.  
86 Furthermore, the warming rate of the TP is heterogeneous both spatially and temporally in recent decades (Duan  
87 & Xiao, 2015; Wu et al., 2015). Under a changing runoff regime (Lin et al., 2020), the lack of a detailed survey  
88 of glacier changes over a long time scale is a major impediment to water resource management and decision-  
89 making (Lutz et al., 2014).

90 The key purpose of this study is therefore to provide an internally consistent dataset of glacier area and mass  
91 change in the WNT over the past 44 years, and comparative analysis of the impact of topography, debris and  
92 proglacial lakes on glacier change during 1976 - 2000 and during 2000 - 2020. Although the area of both debris-  
93 cover and lake terminating glaciers are relatively small, the characteristics of their influence on individual glaciers



94 can be used as a reference for glacier changes in other regions. We have compiled a complete glacier inventory in  
95 the years 1976, 2000, 2014 and 2020 with the Landsat and KH-9 images and quantified the geodetic glacier mass  
96 balance during 1976–2000 and 2000–2020 with DEMs derived from KH-9, ASTER and SRTM3.0. We report area  
97 and mass changes for periods 1976 to 2000 and from 2000 to 2020, and we examine and compare the influence  
98 of topographic, climatic and glaciological factors on these changes during 1976-2000 and 2000-2020.

## 99 **2. Materials and methods**

### 100 **2.1 Study area**

101 The WNT range mountain range has a mean slope of 15° and its elevation spanning 4150-7125 m, with an  
102 average of 4930 m in the whole region. Its primary mountain ridge runs 230 km in a southwest–northeast direction,  
103 bounded by the Nam Co basin to the north and the Lhasa River basin to the south (Yao et al., 2010). Nam Co  
104 Lake, the second largest after Selin Co Lake on the TP, is mainly fed by glacier meltwater (Luo et al., 2020; Zhang  
105 et al., 2017). The Lhasa River basin to the southeast is a major branch of the Yarlung Zangbo River and forms part  
106 of the route taken by the warm and humid monsoon airflow into the plateau, making it warmer and wetter than  
107 the Nam Co basin (Luo et al., 2020). The annual air temperature and precipitation in the WNT range from –0.6°C  
108 to 2.8°C and 37 mm to 500 mm, respectively (Yu et al., 2013).

109 Being in a climatic transition zone, the glaciers in this area range from the maritime-influenced glaciers of  
110 Gangrigabu (southeast TP) to the subcontinental and continental-type glaciers of the Tanggula mountains (Li &  
111 Lin, 2017). There are 845 glaciers covering 675.85 km<sup>2</sup> and 15 debris-covered glaciers with a total area of  
112 71.74km<sup>2</sup> (10.61% of the total glacier area in the WNT ) (RGI 6.0) (RGI Consortium, 2017). Of these, only the  
113 small, ~3km<sup>2</sup> Zhadang and Gurenhekou glaciers (red polygon in Figure 1) have in-situ observations available to  
114 validate the satellite observations, and these run from 2005 to 2010 (Yao et al., 2012).

## 115 **2.2 Methods and data**

### 116 **2.2.1 Glacier outlines**

117 We identified glacier boundaries mainly from Landsat MSS/ETM+/OLI scenes from various years (Table  
118 S1), orthorectified automatically by the USGS using the level 1T SRTM3 DEM (from <http://glovis.usgs.gov/>). We  
119 selected high-quality images with minimal cloud and snow coverage between June and November and used a  
120 semi-automated approach with a TM3/TM5 band ratio ( $2.0 \pm 0.2$ ) to produce glacier outlines. This method is  
121 widely used and appropriate for glacier mapping over large study areas (Guo et al., 2015; Ye et al., 2017). We  
122 used a  $3 \times 3$  median filter to eliminate isolated pixels and likely to have been misclassified due to debris or  
123 boulders on the glacier (Bolch et al., 2010). We manually checked and edited the glacier outlines, including the



124 debris-covered glaciers, with height change maps and a coherence map formed by Sentinel-1 images observed on  
125 2016-08-05 and 2016-08-29, to help distinguish debris-covered ice from ice-free areas. Finally, referring to the  
126 second glacier inventory, we assigned contiguous ice masses to drainage basins in order to obtain a glacier  
127 inventory.

### 128 **2.2.2 Glacier elevation change**

129 We used the KH-9 images and SRTM DEM (version 3) to estimate glacial elevation changes for the period  
130 1976 to 2000, and ASTER DEMs for the period 2000-2020.

#### 131 2.2.2.1 DEM data

132 The declassified KH-9 images were obtained by the Hexagon mission from 1971 to 1986, with a ground  
133 resolution of 6 to 9 m (Surazakov & Aizen, 2010). We downloaded images from 1976-01-07 via the Earth Explorer  
134 user interface (<https://earthexplorer.usgs.gov>) and adopted the Hexagon Imagery Automated Pipeline method to  
135 generate digital elevation models. This method is coded in MATLAB and uses the OpenCV library for Oriented  
136 FAST and Rotated BRIEF (ORB) feature matching, uncalibrated stereo rectification, and semiglobal block  
137 matching algorithms (Maurer & Rupper, 2015).

138 The SRTM mission carried out in February 2000 produced two types of DEM datasets, the C-band DEM  
139 with a coverage range of 60°N ~ 60°S and the X- band DEM with a smaller coverage. We used version 3 of the  
140 C-band SRTM DEM (<https://earthexplorer.usgs.gov/>) at 1-arc-second resolution (about 30 m) in our primary  
141 processing and masked out areas with gaps in the unfilled SRTM3 version 2.1 DEM at 3-arcsecond resolution  
142 (about 90 m).

143 The ASTER instrument was launched on the Terra satellite in December 1999 and a single DEM covers  
144 approximately 3600 km<sup>2</sup>. We downloaded 250 'Data1.13a.demzs' ASTER DEMs at 30 m resolution in geotiff  
145 format with cloud coverage of less than 40% from the METI AIST Data Archive System (MADAS) satellite data  
146 retrieval system (<https://gbank.gsj.jp/madas>). After cloud and outlier removal we fitted a linear regression through  
147 the time series of co-registered ASTER DEMs and set the minimum stack interval per pixel to 15 years to estimate  
148 the rate of elevation change for each 30-m pixel (Maurer et al., 2019).

#### 149 2.2.2.2. Co-registration and bias correction of DEMs

150 All DEMs were co-registered to the SRTM master DEM using a standard elevation–aspect optimization  
151 procedure (Nuth & Kääb, 2011). Then, the elevation correlation deviation of all the DEMs was corrected by a  
152 third-order polynomial. In addition, we used a 2km buffer zone around the union of glacier boundaries to define  
153 stable (unchanging) terrain for DEM alignment, bias correction and uncertainty calculation. Figure. S1a shows  
154 the coverage of the KH-9 images and the number of valid ASTER DEMs grids after removal of clouds and outliers



155 in the buffer. The glacier area covered by the dataset from 1976 to 2000 and from 2000 to 2020 accounted for  
156 70.85% and 81.94% of the total glacier area, respectively (shown in Figure. S1b, c). We used only the area  
157 common to both of these datasets to measure elevation change between the 1976-2000 and 2000-2020 periods.  
158 After correction for alignment and elevation-related deviation, apparent elevation changes over stable terrain  
159 (masked glaciers and lakes in square buffer zone) had no zero change trend with elevation, slope and aspect, as  
160 shown in Figure. S2.

#### 161 2.2.2.3. SRTM Penetration depth correction

162 Over the WNT, the average penetration depth of C-band SRTM is  $1.67 \pm 0.53$  m calculated using X- band  
163 SRTM DEM as the reference (Li & Lin, 2017). Linear regression between the glacier elevation and penetration  
164 showed that the penetration depth varies from 1.29 m to 2 m at altitudes of 5550 m and 6250m respectively (Li &  
165 Lin, 2017). We used this more accurate linear altitude-dependent correction and the result is similar to several  
166 other study regions on the TP (Gardelle et al., 2013; Kääb et al., 2012).

#### 167 2.2.2.4 Glacier mass change

168 Estimation of average glacier thickness changes based on elevation difference maps involves noise filtering  
169 and glacier-hypsometry-weighted averages in an approach widely employed in to calculate regional glacier mass  
170 balance where glacier thinning is highly dependent on altitude. Firstly, we subjected the thickness change maps  
171 to outlier removal using a  $5 \text{ m a}^{-1}$  threshold. We then masked slopes  $> 40^\circ$ , where uncertainties are large (Figure  
172 S2b, c), before visually inspecting the final thickness change maps. We additionally masked out any remaining  
173 anomalous pixels, which occurred almost exclusively in low-contrast, snow-covered accumulation zones. Finally,  
174 we separated thickness changes into 50-m elevation bins by referring to the SRTM at different spatial scales, i.e.,  
175 the whole glacierized area, sub-regions, different glacier types and individual glaciers of area  $> 2 \text{ km}^2$ . In each  
176 altitude bin, we filtered out any height-change values that differed by more than three standard deviations from  
177 the median and removed any bins with less than 100 pixels. For elevation bins with no observations (mostly over  
178 the low- and high- elevation limits), we assumed zero mean elevation changes. We calculated the mean glacier  
179 thickness changes for the spatial unit/group ( $dh$ ) as a hypsometric average:

$$180 \quad dh = \sum_{i=1}^n \frac{S_i}{S} \cdot \overline{dh}_i \quad (1)$$

181 where  $i$  and  $n$  denote the  $i^{\text{th}}$  50-m elevation bin and the number of total bins respectively,  $S_i$  is the glacier area of  
182 the  $i^{\text{th}}$  elevation bin,  $S$  is the total glacier area, and  $dh_i$  is the mean  $dh$  in the bin.

183 We calculated the final geodetic mass balance ( $B$ ) using equation (2).



$$B = dh \times \frac{\rho_{ice}}{\rho_{water}} \quad (2)$$

We translated glacier thickness changes into mass balance by the ratio of column-averaged glacier density,  $\rho_{ice}$  (850 kg m<sup>-3</sup>) to water density ( $\rho_{waters}$ , 1000 kg m<sup>-3</sup>).

### 2.2.3 Uncertainty

#### 2.2.3.1 Uncertainty of glacier area

Similar to previous studies (Wu et al., 2016; Ye et al., 2017), we obtained the uncertainty of glacier area ( $\delta_s$ ) using equation (3)

$$\delta_s = L_c E_{pc} + L_d E_{pd} \quad (3)$$

Where  $L_c$  and  $L_d$  represent the lengths of the clean-ice and debris-covered glacier outlines, and  $E_{pc}$  and  $E_{pd}$  denote the positional accuracies. We calculated the uncertainty in glacier area change ( $\delta_{sc}$ ) by combining the area uncertainties using equation (4)

$$\delta_{sc} = \sqrt{(\delta_{s1})^2 + (\delta_{s2})^2} \quad (4)$$

Guo et al. (2015) compared glacier outlines derived from Landsat-images with real-time kinematic differential GPS (RTK-DGPS) measurements and found an average difference of  $\pm 11$  m and  $\pm 30$  m for the delineation of clean and debris-covered ice. Using a buffer size of 10 m for areas from the Hexagon images (Bolch et al., 2010), our combined uncertainty in glacier area is 3.9%, 5.1%, 5.1% and 5.9% in 1976, 2000, 2014, and 2020, respectively.

#### 2.2.3.2 Uncertainty of glacier thickness change

The uncertainty in surface-elevation change derived from ASTER DEMs can be estimated using the point elevation error ( $E_{pt}$ ) and extrapolation error ( $E_{ext}$ ) (Nuth et al., 2010; Maurer et al., 2016).

$$\delta_{hi} = \sqrt{\left(\frac{E_{pt}}{\sqrt{n_i}}\right)^2 + \left(\frac{E_{ext}}{\sqrt{n_i}}\right)^2} \quad (5)$$

$$n_i = \frac{n_{ib} * r^2}{\pi * d^2} \quad (6)$$

$$\delta_h = \sqrt{\sum_{i=1}^{i=n} (\delta_{hi} * \frac{S_i}{S})^2} \quad (7)$$

Here,  $E_{pt}$  refers to the standard deviations of the relative elevation change over the off- glacier areas,  $E_{ext}$  is the standard deviations of glacial elevation change within each 50-m bin,  $n_{ib}$  and  $n_i$  represent the total number of pixels and the number of independent measurements of pixels respectively,  $r$  is the DEM spatial resolution (30 m in our



210 study), and  $d$  is the autocorrelation length. We used an autocorrelation length of 500 m was employed, which is a  
211 conservative value based on semivariogram analysis of mountainous regions in previous studies (Brun et al., 2018;  
212 Maurer et al., 2019). We combined, the uncertainty of surface-elevation changes derived from the KH-9 DEM  
213 with the SRTM penetration uncertainty, estimated as  $\pm 0.53$  m (Li & Lin, 2017). This study ignored the errors  
214 caused by seasonal changes in glacier thickness due to the lack of observations of such seasonal changes.

215 We estimated the overall uncertainty in the total glacier mass change ( $\delta m$ , in kg) by including the uncertainty  
216 in the assumed ice/firn/snow density ( $\delta \rho = 60$  kg m<sup>-3</sup>, which is 7.1% of  $\rho_{ice} = 850$  kg m<sup>-3</sup>), errors in glacier area  
217 ( $\delta S$ , m<sup>2</sup>) and glacier elevation change ( $\delta h$ , m), using equation (8).

$$\delta_m = \sqrt{(S \cdot dh \cdot \delta_\rho)^2 + (\delta_s \cdot dh \cdot \rho_{ice})^2 + (S \cdot \delta_h \cdot \rho_{ice})^2} \quad (8)$$

#### 219 2.2.4. Lake data

220 We identified glacier-marginal lakes as those lying within 50 m of a glacier boundary, using lake data for the  
221 1970s-2018 (Luo et al., 2020; <http://data.tpdc.ac.cn>).

#### 222 2.2.5. Meteorological data

223 There are three meteorological stations adjacent to the WNT, at Bange (31°23'N, 90°01'E), Lhasa (29°40'N,  
224 91°08'E), and Damxung (30°29'N, 91°06'E). We obtained air temperature and precipitation data during 1976-  
225 2020 from the Climatic Data Center, National Meteorological Information Center, of the China Meteorological  
226 Administration.

227 We also obtained gridded data of precipitation and temperature with spatial resolution of  $0.1^\circ \times 0.1^\circ$  and 3-  
228 h time interval for 1979-2018 from the China Meteorological Forcing Data (Ding et al., 2020;  
229 <http://data.tpdc.ac.cn>), which has been widely utilized in land-process, hydrological modelling, and other studies  
230 (Qiao et al., 2021; Wang et al., 2020, 2021). This dataset is made by fusing the conventional meteorological  
231 observation of China Meteorological Administration based on the Princeton reanalysis data, GLDAS data,  
232 GEWEX-SRB radiation data, and TRMM precipitation data as the background field (He et al., 2020; Yang et al.,  
233 2010).

### 234 3. Results

#### 235 3.1 Glacier area change

236 There were 921 glaciers with a total area of  $589.17 \pm 31.72$  km<sup>2</sup> in 2020 in the WNT (Figure 2a). Small  
237 glaciers dominated the number (those  $\leq 1$  km<sup>2</sup> occupy 83.17% of the total number) and a large proportion of the





238 area (those  $\leq 1$  km<sup>2</sup> occupy 30.42% of the total area). Glaciers larger than 5 km<sup>2</sup> accounted for 21.39% of the total  
239 area and only 1.63% of the total number. Glaciers were mainly distributed in the eastern-oriented zone with an  
240 altitude of 5600-6100m and a slope of 5-40° (Figure 2b, c, d).

241 Glaciers in the WNT experienced significant retreat from 1976 to 2020 and altitude, slope and aspect all  
242 appear to have influenced this retreat (Figures 3 and 4). The glacier area decreased by 33.42% from 884.90 ±  
243 29.71 km<sup>2</sup> in 1976 to 589.17 ± 31.72 km<sup>2</sup> in 2020, with an average annual decrease of  $-0.76 \pm 0.11$  % a<sup>-1</sup>. The  
244 retreat rate of glacier area in 2000-2020 ( $-1.17\%$  a<sup>-1</sup>) was more than twice as fast as in 1976-2000 ( $-0.54 \pm 0.21$  %  
245 a<sup>-1</sup>) (Figure 4, Table 1). The glacier area declined faster in the northeast and southwest but slower in the middle,  
246 except for a few small glaciers with an area of less than 2 km<sup>2</sup> during 1976-2000. During 2000-2020 the glacier  
247 area receded faster in the whole region except for a few small glaciers with an area of less than 1 km<sup>2</sup> (Figure 3).  
248 Retreat was greatest in the area classes of 1-3 km<sup>2</sup> and 3-5 km<sup>2</sup>, and glaciers with significant areal retreat were  
249 mainly distributed below 6,000 m altitude. Glaciers in the Nam Co basin retreated slightly faster than those outside  
250 this basin between 2000 and 2020. Retreat was particularly rapid at lower altitudes and decreased at higher  
251 elevations. As for the effect of slope and aspect, glacier retreated more rapidly with increasing slope between 5°  
252 and 40°, but the retreat rate decreased as slope increased between 0°-5° and 40°-60°, where relative few glaciers  
253 are distributed. During both 1976-2000 and 2000-2020, the retreat rate was smallest on the north-facing slopes.  
254 During 1976-2000, retreat was most rapid in the southeast quadrant, while from 2000 to 2020, rapid retreat  
255 occurred at similar rates in all aspects other than north and southeast, i.e., the effect of aspect on glacier area retreat  
256 varied in space and time.

### 257 3.2 Geodetic mass balance

258 Glacier height changes for the past 44 years, are shown in Figure 5. Substantial and near-ubiquitous thinning  
259 occurred in the WNT since 1976, with a widespread increase in the most recent decades. From 1976 to 2000,  
260 glaciers experienced a mean elevation rate of  $-0.31 \pm 0.10$  m a<sup>-1</sup> (a water-equivalent loss rate of  $-0.26 \pm 0.09$  m  
261 w.e. a<sup>-1</sup>) equating to a mass loss rate of  $-0.24 \pm 0.08$  Gt a<sup>-1</sup>. From 2000 to 2020, the mean elevation rate was  $-0.44$   
262  $\pm 0.13$  m a<sup>-1</sup>, ( $0.37 \pm 0.12$  m w.e. a<sup>-1</sup>) or  $-0.29 \pm 0.09$  Gt a<sup>-1</sup>. Several glacier tongues have suffered severe thinning,  
263 exceeding  $-1.5$  m a<sup>-1</sup> from 1976 to 2000, notably several long, debris-free glaciers on the south-western slope.  
264 From 2000 to 2020, the range of glacier tongues with losses exceeding 1.5 m a<sup>-1</sup> expanded, and losses were greater  
265 in the north-eastern WNT (see, the red rectangular box in Figure 5). In both 1976-2000 and 2000-2020, the glacier  
266 thinning rate was slightly higher inside the Nam Co drainage basin than outside it (Table 2, Figure. 6), though  
267 these rates do not differ by more than their combined uncertainties.

268 For glaciers with an area of more than 2 km<sup>2</sup>, we found high loss rates in the northeast, followed by the



269 southwest, and moderate in the middle during 2000-2020, but there no obvious spatial varied trend of mass loss  
270 during 1976-2000 (Figure 7). Mass loss was substantially more intense in 2000-2020 with no glaciers in a state  
271 of positive balance (Figure 7, blue dots) and loss from some glaciers in the northeast exceeded  $-0.6 \text{ m w.e. a}^{-1}$ .  
272 Moreover, we found that glacier area retreat and mass loss was not synchronized between the two periods 1976-  
273 2000 and 2000-2020. The glacier with the fastest area retreat did not correspond to the glacier with the fastest  
274 mass decrease, and the spatial varied trend of glacier area retreat rate was inconsistent with that of mass loss rate  
275 (Figure 4 and 9).

276 Finally, glacier elevation change as a function of elevation slope and aspect are shown in Figure 8. Elevation  
277 is inversely correlated with thickness change, while slope and aspect appear to have a weak relationship with  
278 thickness change. In both 1976-2000 and 2000-2020, the elevation change rate was the largest at lower altitudes,  
279 and gradually decreased with the increasing of altitude. The thinning rate also exhibited a weak inverse  
280 relationship with slope, becoming somewhat stronger in the 2000-2020 period. For the impact of aspect, thinning  
281 for 1976-2000 was most rapid in the south-west and north-west quadrants, but by 2000-2016 high thinning rates  
282 were affecting all aspects, i.e., the effect of aspect on thinning rates also varied through time.

### 283 3.3 The effect of debris-cover and proglacial lakes on glacier mass changes

284 In our WNT study area, there are five debris-covered glaciers, covering  $55.42 \pm 1.25 \text{ km}^2$  in 1976 and  $51.59$   
285  $\pm 1.77 \text{ km}^2$  in 2000. Lake-terminating glaciers occupied a similar proportion, with area of  $70.29 \pm 2.69 \text{ km}^2$  in  
286 1976, and  $49.60 \pm 1.82 \text{ km}^2$  in 2000. Only one glacier was both covered by debris and terminated in a pro-glacial  
287 lake.

288 The thinning rate of different types of glaciers varied somewhat, though with greater uncertainty given the  
289 relatively small sample. (Figure 9, Table 3). During 1976-2000, the lake-terminating glaciers thinned more rapidly,  
290 followed by the regular and debris-covered glacier types. From 2000 to 2020, the ablation rate of debris-covered  
291 glaciers was slightly lower than that of regular glaciers at low altitudes, but progressively greater at higher altitudes,  
292 leading to a slightly more negative total mass balance for the debris-covered type. In the same period, the thinning  
293 of lake-terminating glaciers continued to exceed that of regular glacier. Our results suggest that debris cover in  
294 the WNT suppressed glacier thinning to some extent and enabled the debris-covered ice to survive at lower  
295 elevations than adjacent clean ice glaciers. In contrast, a glacial lake at the end of a glacier accelerated its retreat,  
296 and this behavior was more pronounced at lower elevations.



297 **4. Discussion**

298 **4.1 Comparison to previous studies**

299 **4.1.1 Glacier area change**

300 Based on space-borne imagery, we found that glacier area in the west Nyainqentanglha Range (WNT) has  
301 changed by -13.0% from 1976 to 2000 and -23.5% from 2000 to 2020. The comparison between this and previous  
302 studies is shown in Tables S2 and S3. Differences between studies may have arisen from the georeferencing errors  
303 in the areas for 1970 used by Shangguan et al. (2008) and Wu & Zhu (2008) which came from the Chinese Glacier  
304 Inventory (CGI) based on the Chinese topographic maps (Frauenfelder & Kääb, 2009). Although obvious errors  
305 in the CGI were omitted in their change analysis, the remaining glaciers were not corrected (Frauenfelder & Kääb,  
306 2009). Discrepancies may also have arisen from differences in the methods used to distinguish glaciers from  
307 seasonal snow, and debris-cover glaciers from neighboring moraine or rock slopes (Bolch et al., 2010). Compared  
308 to the glacier-area change between 1970-2000 and 2000-2014 of Wu et al. (2016), and between 1977-2000 and  
309 2000-2010 of Wang et al. (2012), our results agree within the uncertainties over the whole WNT, and the southeast  
310 WNT respectively. In addition, the 789.15 km<sup>2</sup> area reported for the WNT by RGI V4.0 which used Landsat images  
311 obtained on 2001-12-06 agrees with our result. 4.1.2 Glacier mass balance.

312 **4.1.2 Glacier mass balance**

313 Field measurements of mass balance are available from small Zhadang glacier for 2005-2008, and  
314 Gurenhekou glacier for 2005-2010 on the southeastern slope of the WNT (Table S4). Although the period of our  
315 study is longer and provides a much larger sample size, the mass balance results are similar to these field  
316 measurements.

317 Previous studies have also reported region-averaged glacier mass balance over a similar spatial extent to ours,  
318 obtained from DEMs using various sensors (Table S5). Our results during 2000-2020 are more negative than those  
319 of Neckel et al. (2014), Li & Lin (2017) and Zhang & Zhang (2017), but agree within the uncertainties over  
320 comparable time periods, even though these studies differ in data processing, glacier mask, penetration correction  
321 and data coverage. For comparison, we calculated the change for the 2000-2014 period from ASTER DEMs  
322 (Figure 10). Our estimated mass balance in this area ( $-0.28 \pm 0.15$  m w.e. a<sup>-1</sup>) is very similar to the other studies  
323 (Table S5). It is also similar to that of 1976-2000, suggesting that the more strongly negative average for the longer  
324 2000 to 2020 period ( $-0.37 \pm 0.12$  m w.e. a<sup>-1</sup>) is the result of particularly strong negative mass balance after 2014,  
325 although cloud-free ASTER data are insufficient for direct calculation of the mass balance from 2014-2000. This  
326 interpretation is supported by Ren et al. (2020) who also calculated a higher 2013-2020 thinning rate ( $-0.43 \pm 0.06$



327 m w.e. a<sup>-1</sup>) twice as negative as in 2000-2013. Though the difference in rate is within the combined uncertainties  
328 for these periods, this apparent acceleration in thinning in WNT (from  $-0.26 \pm 0.06$  m w.e. a<sup>-1</sup> in 1976-2000 to -  
329  $0.37 \pm 0.15$  m w.e. a<sup>-1</sup> in 2000-2020), is similar to the broader regional pattern of accelerating loss across the  
330 Himalayas and Kangri Karpo Mountains (Maurer et al., 2019; Wu et al., 2018, 2019).

#### 331 **4.2 The influences of debris-cover and proglacial lakes on glacier mass changes**

332 Debris can inhibit or enhance glacial ablation depending on its thickness (Maurer et al., 2016). A shallow  
333 layer of debris usually enhance melt rates due to its low surface albedo, while thicker layers could suppress melt  
334 rates through thermal insulation (Reid et al., 2012). Our results (Table 3) suggest that the debris-covered glaciers  
335 in our study thinned more slowly than the regular, debris-free glaciers in the 1976-2000 period, though the  
336 difference is not statistically significant and the small sample size (5) of the debris-covered glaciers compared to  
337 regular glaciers (>600) limits our ability to compare these classes. In the 2000-2020 period, the thinning rate of  
338 the debris-covered glaciers increased significantly, to double its previous rate, though it remains indistinguishable  
339 from the thinning rate for regular glaciers at that time. While several previous studies indicated that on the glacier-  
340 scale, debris-covered glaciers thin more slowly than debris-free glaciers (Nicholson & Benn, 2006; Scherler et al.,  
341 2011; Vincent et al., 2016), large-scale geodetic studies reported no significant differences in the thinning rates  
342 between debris-covered and clean glaciers on time scales more than a decade after 2000 (Brun et al., 2019; Ke et  
343 al., 2020; Maurer et al., 2019), a finding that is supported by this study.

344 Banerjee (2017) suggested that the thinning rate of a debris-covered glacier is initially slower than that of a  
345 similar clean glacier at the early stage of warming but subsequently matches and then overtakes the clean  
346 counterpart. In this theory, the time required for their respective melting rates to cross is controlled by the rate of  
347 warming, with little difference between their thinning rates at low rates of warming (Banerjee, 2017). The large  
348 difference in the 1976-2000 mean melt rates of the regular versus debris-covered glaciers in our study provides  
349 some supports for this theory, but a larger sample with lower uncertainty is needed to verify this.

350 Glaciers with proglacial lakes can experience relatively high mass loss through calving and thermal  
351 undercutting (Maurer et al., 2016; Thompson et al., 2012) and the expansion of such lakes can cause dynamic  
352 thinning to propagate up-glacier (Ke et al., 2020). Glaciers terminating in proglacial lakes in our study area had  
353 the highest mean thinning rates of all the classes in both time periods, and more negative mass balance compared  
354 to both regular and debris covered glacier during 2000-2020.

#### 355 **4.3 Topographic and climatic controls of varying glacier mass loss**

356 If climate is the driving force behind glacier change, topographical parameters can modulate this change



357 (Pandey et al., 2017). Controls on glacier thickness and areal change are complicated, however, with additional  
358 factors including local variations in climate, glacier thickness, morphology, the presence of proglacial/supraglacial  
359 lakes and debris cover, and latitude and longitude (Brun et al., 2018,2019; Ke et al.,2020; Maurer et al., 2019).

360 We found that both glacier areal retreat rate (Figure 5b) and thinning rate (Figures 5 and 7) generally  
361 decreased with increasing altitude, agreeing with previous studies (Li & Lin, 2017; Wu et al., 2016; Ye et al., 2017;  
362 Zhou et al., 2019). However, the effect of slope and aspect on glacier thickness has been rarely studied. We found  
363 that in the slope range of 8-40°, where the glaciers were mainly distributed, the rate of areal retreat increased as  
364 slope increased (Figure 3c), but the thinning rate decreased (Figure 7b). This may reflect the preferential loss  
365 (retreat) of relative thin ice on steeper slopes, even where thinning rates were not exceptional. Overall, the  
366 relationship between aspect and both areal retreat and thinning was spatially inconsistent and varied in time  
367 (Figures 3d and 7c).

368 Mean glacier mass thinning and retreat rates were consistently higher in the Nam Co basin than Lhasa River  
369 basin (Table 1 and 2), in agreement with Bolch et al.(2010) and Li & Lin (2017), and the glaciers in central WNT  
370 showed particularly strong melting from 2000 to 2020. While the glacier distribution on the TP broadly follows  
371 the regional atmospheric circulation pattern (Yao et al., 2012), the variability in glacier loss within regions cannot  
372 always be fully explained by the changes in precipitation and temperature on this scale (Wu et al., 2018).

373 The increasingly-negative mass balance through time is consistent with the temperature record from the  
374 three weather stations that shows a consistent warming trend (averaging 0.0485 °C a<sup>-1</sup>) (Figure 11) and gridded  
375 temperature data showing a more rapid increase during 2000-2018 than 1979-2000 (Figure 12), alongside  
376 precipitation that increased during 1979-2020 but decreased during 2000-2018. The accelerated warming from  
377 2014 to 2018 (red area in Figure 11 (2014-2018)) corresponds geographically to the substantial central-WNT  
378 glacier thinning highlighted in the red rectangle in Figure 5. Precipitation also increased substantially in this region  
379 from 2014 to 2018, and glacier melting can be particularly intense under combined warm and wet conditions (Li  
380 et al., 2020; Oerlemans & Fortuin, 1992).

381 While the overall, the trends of temperature and precipitation in the ablation season (June to September)  
382 and accumulation season (October to December and January to May) were similar to annual changes, the  
383 temperature and precipitation data from 2014 to 2018 described above offer a compelling explanation for the main  
384 temporal and spatial variations in glacier change in the WNT, particularly the high rates of thinning from 2014-  
385 2018. They do not directly explain why the Nam Co glaciers thinned more rapidly than elsewhere, however.

386 The area-weighted mean glacier elevation in the Nam Co basin is slightly lower than that of Lhasa River  
387 basin (Figure S1), which may help explain this, though even in some comparable elevation bins, the Nam Co rates



388 were more negative than equivalent Lhasa-basin rates (Figure 6). Other possible explanations include difference  
389 in the impact of black carbon and dust in reducing surface albedo (Lau et al., 2010; Ming et al., 2008), and Qu et  
390 al. (2014) did observe a decrease in albedo at Zhadang glacier (Nam Co drainage basin) from 2001-2012.

## 391 **5. Conclusions**

392 Based on KH-9, Landsat, SRTM and ASTER satellite data, we have quantified the changes of glacier area,  
393 surface elevation and mass balance in the WNT over the past 44 years and compared the effects of topography,  
394 debris-cover and proglacial lakes on glacier change during 1976-2000 and 2000-2020. Our major conclusions are:

395 (1) Glaciers in the WNT retreated by  $295.73 \pm 43.45 \text{ km}^2$ , or  $33.42 \pm 4.9\%$  of their area, from 1976-2020, at  
396 a mean rate of  $-0.76 \pm 0.11 \text{ \% a}^{-1}$ . Over this time, they lost a total of  $11.56 \pm 0.12 \text{ Gt}$  of ice.

397 (2) The average retreat rate from 2000 to 2020 ( $1.17 \pm 0.30 \text{ \% a}^{-1}$ ) was more than twice that from 1976 to  
398 2000 ( $0.54 \pm 0.21 \text{ \% a}^{-1}$ ). Similarly, the mean glacier mass balance from 2000 to 2020 ( $-0.37 \pm 0.12 \text{ m w.e.a}^{-1}$ )  
399 was more negative than that from 1976 to 2000 ( $-0.26 \pm 0.09 \text{ m w.e.a}^{-1}$ ) (though the change is within the  
400 uncertainties). The more rapid ice loss from 2000 to 2020 was mainly due to intensified glacier melting after 2014,  
401 which was likely associated with particularly strong warming of the region after that year. Besides, areal retreat  
402 rate and mass loss rate of most glaciers was not synchronized during 1976-2000 and 2000-2020.

403 (3) In the WNT the spatial and temporal patterns of glacier loss can largely be explained by the observed  
404 patterns of regional climate change. Locally, the mass balance varied between different types of glaciers with  
405 proglacial lakes associated with the most rapid loss, particularly during 2000-2020. The mass balance of debris-  
406 covered glaciers was similar to debris-free glaciers during 2000-2020.

407 (4) Topographic setting influenced retreat and thinning, with loss rates decreasing with increasing elevation.  
408 The rate of both glacier retreat and thinning decreased with elevation, but the relationship between the parameters  
409 of slope and aspect with thinning rates differed from their relationship with retreat rates, spatially and through  
410 time. For slopes of  $8\text{-}40^\circ$  (which includes most glaciers), for example, the retreat rate increased with slope while  
411 the thinning rate decreased.

412 In this study, we observed accelerated glacier loss in the WNT on multi-year time scales. However, factors  
413 such as precipitation, temperature and altitude could not yet fully explain the heterogeneity of glacier changes.  
414 Thus, more detail data and glacier ablation models are needed to fully understand the mechanism of glacier change  
415 in the future.

## 416 **Author contributions:**

417 Conceptualization, S.W. and J.L.; methodology, S.W.; software, S.W. and X.Q.; data curation, S.W., and J.Z;



418 writing—original draft preparation, S.W.; writing—review and editing, H.P. and L.K.; visualization, H.P. and J.L.;  
419 supervision, W.X. and Y.Z.; project administration, J.L.; funding acquisition, J.L.

#### 420 **Acknowledgements:**

421 This work was supported by the Second Tibetan Plateau Scientific Expedition and Research Program (STEP;  
422 Ministry of Science and Technology, MOST; grant no. 2019QZKK0207), the National Natural Science  
423 Foundation of China (NSFC; grant no. 92047301).

#### 424 **References:**

425 Bahr, D. B., Meier, M. F., & Peckham, S. D.: The physical basis of glacier volume-area scaling, *J Geophys Res-*  
426 *Sol Ea*, 102(B9), 20355–20362, <https://doi.org/10.1029/97JB01696>, 1997.

427 Bahr, D. B., Pfeffer, W. T., & Kaser, G.: A review of volume-area scaling of glaciers, *Rev Geophys*, 53(1), 95–  
428 140. <https://doi.org/10.1002/2014RG000470>, 2015.

429 Banerjee, A.: Brief communication: thinning of debris-covered and debris-free glaciers in a warming climate,  
430 *Cryosphere*, 11(1), 133–138. <https://doi.org/10.5194/tc-11-133-2017>, 2017.

431 Bolch, T., Yao, T., Kang, S., Buchroithner, M. F., Scherer, D., & Schneider, C., et al.: A glacier inventory for the  
432 western Nyainqentanglha range and the Nam Co Basin, Tibet, and glacier changes 1976–2009, *Cryosphere*, 4(3),  
433 419–433, <https://doi.org/10.5194/tc-4-419-2010>, 2010.

434 Brun, F., Berthier, E., Wagnon, P., Kääb, A., & Treichler, D.: A spatially resolved estimate of High Mountain Asia  
435 glacier mass balances, 2000–2016. *Nat Geosci*, 10(9), 668–673, <https://doi.org/10.1038/s41561-018-0171-z>, 2018.

436 Brun, F., Wagnon, P., Berthier, E., Jomelli, V., Maharjan, S. B., & Kraaijenbrink, P. D. A., et al.: Heterogeneous  
437 Influence of Glacier Morphology on the Mass Balance Variability in High Mountain Asia, *J Geophys Res-Sol Ea*,  
438 124(6), 1331–1345, <https://doi.org/10.1029/2018JF004838>, 2019.

439 Brun, F., Wagnon, P., Berthier, E., Shea, J. M., & Immerzeel, W. W.: Ice cliff contribution to the tongue-wide  
440 ablation of Changri Nup Glacier, Nepal, central Himalaya, *Cryosphere*, 12(11), 3439–3457,  
441 <https://doi.org/10.5194/tc-12-3439-2018>, 2018.

442 Ding, L., Zhou, J., Wang, W.: Dataset of 0.01° Surface Air Temperature over Tibetan Plateau (1979–2018),  
443 National Tibetan Plateau Data Center, 10.11888/Meteoro.tpd.c.270339. CSTR: 18406.11.Meteoro.tpd.c.270339,  
444 2020.

445 Duan, A., & Xiao, Z.: Does the climate warming hiatus exist over the Tibetan Plateau? *Sci Rep-UK*. 5, 13711,  
446 <https://doi.org/10.1038/srep13711>, 2015.

447 Frauenfelder, R., & Kääb, A.: Glacier mapping from multi-temporal optical remote sensing data within the



- 448 Brahmaputra River Basin, In Proceedings of the 33rd International Symposium on Remote Sensing of  
449 Environment, 4-8, 2009.
- 450 Gardner, A. S., Moholdt, G., Cogley, J. G., Wouters, B., Arendt, A. A., Wahr, J., et al.: A reconciled estimate of  
451 glacier contributions to sea level rise: 2003 to 2009, *Science*, 340(6134), 852-857,  
452 <https://doi.org/10.1126/science.1234532>, 2013.
- 453 Guo, W., Liu, S., Xu, J., Wu, L., Shangguan, D., & Yao, X., et al.: The second chinese glacier inventory: data,  
454 methods and results, *J Glaciol.* 61(226), 357-372, <https://doi.org/10.3189/2015JoG14J209>, 2015.
- 455 He, J., Yang, K., Tang, W., Lu, H., Qin, J., & Chen, Y., et al.: The first high-resolution meteorological forcing  
456 dataset for land process studies over China, *Sci Data*, 7, <https://doi.org/10.1038/s41597-020-0369-y>.
- 457 Kääb, A., Berthier, E., Nuth, C., Gardelle, J., & Arnaud, Y.: Contrasting patterns of early twenty-first-century  
458 glacier mass change in the Himalayas, *Nature*, 488(7412), 495-498, <https://doi.org/10.1038/nature11324>, 2012.
- 459 Ke, L., Song, C., Yong, B., Lei, Y., & Ding, X.: Which heterogeneous glacier melting patterns can be robustly  
460 observed from space? A multi-scale assessment in southeastern Tibetan Plateau, *Remote Sens Environ*, 242,  
461 <https://doi.org/10.1016/j.rse.2020.111777>, 2020.
- 462 Lau, W., Kim, M. K., Kim, K. M., & Lee, W. S.: Enhanced surface warming and accelerated snow melt in the  
463 Himalayas and Tibetan Plateau induced by absorbing aerosols, *Environ. Res. Lett.*, 5(2), 025204,  
464 <https://doi.org/10.1088/1748-9326/5/2/025204>, 2010.
- 465 Li, Y. J., Ding, Y.J., Shangguan, D. H., & Wang, R. J.: Regional differences in global glacier retreat from 1980 to  
466 2015 - sciencedirect, *Adv. Clim. Chang. Res.*, 10(4), 203-213. <https://doi.org/10.1016/j.accre.2020.03.003>, 2020.
- 467 Li, G., & Lin, H.: Recent decadal glacier mass balances over the Western Nyainqentanglha Mountains and the  
468 increase in their melting contribution to Nam Co Lake measured by differential bistatic SAR interferometry,  
469 *Global Planet Change*, 149, 177-190, <https://doi.org/10.1016/j.gloplacha.2016.12.018>, 2017.
- 470 Lin, L., Gao, M., Liu, J., Wang, J., Wang, S., & Chen, X., et al.: Understanding the effects of climate warming on  
471 streamflow and active groundwater storage in an alpine catchment: The upper Lhasa River, *Hydrol Earth Syst Sc.*  
472 24(3), 1145-1157, <https://doi.org/10.5194/hess-24-1145-2020>, 2020.
- 473 Luo, W., Zhang, G., Chen, W., & Xu, F.: Response of glacial lakes to glacier and climate changes in the western  
474 Nyainqentanglha range, *Sci Total Environ.* 735, 139607, <https://doi.org/10.1016/j.scitotenv.2020.139607>, 2020.
- 475 Lutz, A. F., Immerzeel, W. W., Shrestha, A. B., & Bierkens, M. F. P.: Consistent increase in High Asia's runoff  
476 due to increasing glacier melt and precipitation, *Nat Clim Change*, 4(7), 587-592,  
477 <https://doi.org/10.1038/nclimate2237>, 2014.
- 478 Maurer, J. M., Schaefer, J. M., Rupper, S., & Corley, A.: Acceleration of ice loss across the Himalayas over the





- 479 past 40 years, *Sci Adv.* 5(6), aav7266, <https://doi.org/10.1126/sciadv.aav7266>, 2019.
- 480 Maurer, J., & Rupper, S.: Tapping into the Hexagon spy imagery database: A new automated pipeline for  
481 geomorphic change detection, *ISPRS J Photogramm.* 108, 113-127,  
482 <https://doi.org/10.1016/j.isprs.2015.06.008>, 2015.
- 483 Maurer, J. M., Rupper, S. B., & Schaefer, J. M.: Quantifying ice loss in the eastern himalayas since 1974 using  
484 declassified spy satellite imagery, *Cryosphere*, 10(5), 2203-2215, <https://doi.org/10.5194/tc-10-2203-2016>, 2016.
- 485 Ming, J., Cachier, H., Xiao, C., Qin, D., Kang, S., & Hou, S., et al.: Black carbon record based on a shallow  
486 Himalayan ice core and its climatic implications, *Atmos Chem Phys*, 8(5), 1343-1352,  
487 <https://doi.org/10.5194/acp-8-1343-2008>, 2008.
- 488 Neckel, N., Kropáč, J., Bolch, T., & Hochschild, V.: Glacier mass changes on the Tibetan Plateau 2003 – 2009  
489 derived from ICESat laser altimetry measurements, *Environ Res Lett*, 9(1), 468-475,  
490 <https://doi.org/10.1088/1748-9326/9/1/014009>, 2014.
- 491 Nie, Y., Pritchard, H. D., Liu, Q., Hennig, T., Wang, W., Wang, X., et al.: Glacial change and hydrological  
492 implications in the Himalaya and Karakoram, *Nat. Rev. Earth Environ*, 2(2), 91-106, <https://doi.org/10.1038/s43017-020-00124-w>, 2021.
- 494 Nuth, C., & Kääb, A.: Co-registration and bias corrections of satellite elevation data sets for quantifying glacier  
495 thickness change, *Cryosphere*, 5(1), 271-290, <https://doi.org/10.5194/tc-5-271-2011>, 2011.
- 496 Oerlemans, J., & Fortuin, J.: Sensitivity of Glaciers and Small Ice Caps to Greenhouse Warming. *Science*,  
497 258(5079), 115-117, <https://doi.org/10.1126/science.258.5079.115>, 1992.
- 498 Pandey, P., Ali, S. N., Ramanathan, A. L., Champati ray, P. K., & Venkataraman, G.: Regional representation of  
499 glaciers in Chandra Basin region, western Himalaya, India, *Geosci Front.* 8(4), 841-850,  
500 <https://doi.org/10.1016/j.gsf.2016.06.006>, 2017.
- 501 Pritchard, H. D.: Asia's shrinking glaciers protect large populations from drought stress. *Nature*.569(7758), 649-  
502 654, <https://doi.org/10.1038/s41586-019-1240-1>, 2019.
- 503 Qiao, X., Liu, J., Wang, S., Wang, J., Ji, H., Chen, X., et al.: Lead-lag correlations between snow cover and  
504 meteorological factors at multi-time scales in the Tibetan Plateau under climate warming, *Theor. Appl. Climatol*,  
505 146(3), 1459-1477, <https://doi.org/10.1007/s00704-021-03802-x>, 2021.
- 506 Qu, B., Ming, J., Kang, S. C., Zhang, G. S., Li, Y. W., & Li, C. D. et al.: The decreasing albedo of the Zhadang  
507 glacier on western Nyainqentanglha and the role of light-absorbing impurities, *Atmos Chem Phys*.14(20), 11117-  
508 11128, <https://doi.org/10.5194/acp-14-11117-2014>, 2014.
- 509 Reid, T. D., Carenzo, M., Pellicciotti, F., & Brock, B. W.: Including debris cover effects in a distributed model of



- 510 glacier ablation, *J Geophys Res-Atmos*, 117(D18), <https://doi.org/10.1029/2012JD017795>, 2012.
- 511 Ren, S., Menenti, M., Jia, L., Zhang, J., & Li, X.: Glacier Mass Balance in the Nyainqentanglha Mountains  
512 between 2000 and 2017 Retrieved from ZiYuan-3 Stereo Images and the SRTM DEM, *Remote Sens*, 12(5), 864-,  
513 <https://doi.org/10.3390/rs12050864>, 2020.
- 514 RGI Consortium.: Randolph Glacier Inventory – A Dataset of Global Glacier Outlines: Version 6.0, July, 1–27,  
515 <https://ci.nii.ac.jp/naid/40021243259/>, 2017.
- 516 Scherler, D., Bookhagen, B., & Strecker, M. R.: Spatially variable response of himalayan glaciers to climate  
517 change affected by debris cover, *Nat Geosci*, 4(3), 156-159, <https://doi.org/10.1038/ngeo1068>, 2011.
- 518 Shangguan, D. H., Liu, S. Y., Ding, L. F., Zhang, S. Q., Gang, L. I., & Zhang, Y., et al.: Variation of Glaciers in the  
519 Western Nyainqentanglha Range of Tibetan Plateau during 1970 – 2000, *Journal of Glaciology and Geocryology*,  
520 2008. (In Chinese)
- 521 Su, F., Zhang, L., Ou, T., Chen, D., Yao, T., & Tong, K., et al.: Hydrological response to future climate changes for  
522 the major upstream river basins in the Tibetan Plateau, *Global Planet Change*, 136, 82-95,  
523 <https://doi.org/10.1016/j.gloplacha.2015.10.012>, 2016.
- 524 Surazakov, A., & Aizen, V.: Positional accuracy evaluation of declassified hexagon KH-9 mapping camera  
525 imagery, *Photogramm Eng Rem S*, 76(5), 603-608, <https://doi.org/10.14358/PERS.76.5.603>, 2010.
- 526 Thompson, S. S., Benn, D. I., Dennis, K., & Luckman, A.: A rapidly growing moraine-dammed glacial lake on  
527 Ngozumpa Glacier, Nepal. *Geomorphology*, 145–146, 1–11, <https://doi.org/10.1016/j.geomorph.2011.08.015>,  
528 2012.
- 529 Vincent, C., Wagon, P., Shea, J. M., Immerzeel, W. W., Kraaijenbrink, P., & Shrestha, D., et al.: Reduced melt  
530 on debris-covered glaciers: Investigations from Changri Nup Glacier, Nepal, *Cryosphere*, 10(4), 1845-1858,  
531 <https://doi.org/10.5194/tc-10-1845-2016>, 2016.
- 532 Viviroli, D., Dürr, H. H., Messerli, B., Meybeck, M., & Weingartner, R.: Mountains of the world, - water towers  
533 for humanity: Typology, mapping, and global significance, *Water Resour Res.* 43(7),  
534 <https://doi.org/10.1029/2006WR005653>, 2007.
- 535 Wang, J. R., Chen, X., Liu, J. T., & Qi, H.: Changes of Precipitation–Runoff Relationship Induced by Climate  
536 Variation in a Large Glaciated Basin of the Tibetan Plateau, *J. Geophys. Res.-Atmos*, 126(21),  
537 <https://doi.org/10.1029/2020JD034367>, 2021.
- 538 Wang, Q., Yi, S., & Sun, W.: Continuous Estimates of Glacier Mass Balance in High Mountain Asia Based on  
539 ICESat-1,2 and GRACE/GRACE Follow-On Data, *Geophys Res Lett*, 48(2).  
540 <https://doi.org/10.1029/2020GL090954>, 2021.



- 541 Wang, X., Zhou, A. G., Siegert, F., Zhang, Z., & Chen, K. L.: Glacier temporal-spatial change characteristics in  
542 western Nyainqentanglha Range, Tibetan Plateau 1977-2010, *Earth Science - Journal of China University of*  
543 *Geosciences*, 37(5): 1082-1092, 2012. (In Chinese)
- 544 Wu, G., Duan, A., Liu, Y., Mao, J., Ren, R., & Bao, Q., et al.: Tibetan Plateau climate dynamics: Recent research  
545 progress and outlook, *Natl Sci Rev*, 2(1), 100–116, <https://doi.org/10.1093/nsr/nwu045>, 2015.
- 546 Wu, K. P., Liu, S., Jiang, Z., Xu, J. L., & Wei, J.: Glacier mass balance over the central Nyainqentanglha Range  
547 during recent decades derived from remote-sensing data, *J Glaciol.*65(251), 422–439,  
548 <https://doi.org/10.1017/jog.2019.20>, 2019.
- 549 Wu, K. P., Liu, S., Jiang, Z., Xu, J., Wei, J., & Guo, W.: Recent glacier mass balance and area changes in the  
550 kangri karmo mountains from dems and glacier inventories, *The Cryosphere*. 12(1), 103-121,  
551 <https://doi.org/10.5194/tc-12-103-2018>, 2018.
- 552 Wu, K. Q., Liu, S. Y., Guo, W. Q., Wei, J. F., Xu, J. L., & Bao, W. J., et al.: Glacier change in the western  
553 Nyainqentanglha Range, Tibetan Plateau using historical maps and Landsat imagery: 1970-2014, *J MT Sci Engl*,  
554 13(8), 1358–1374, <https://doi.org/10.1007/s11629-016-3997-0>, 2016.
- 555 Wu, Y., & Zhu, L.: The response of lake-glacier variations to climate change in Nam Co Catchment, central  
556 Tibetan Plateau, during 1970–2000, *J Geogr Sci*, 18(2), 177-189, <https://doi.org/10.1007/s11442-008-0177-3>,  
557 2008.
- 558 Yang, K., He, J., Tang, W., Qin, J., & Cheng, C.: On downward shortwave and longwave radiations over high  
559 altitude regions: Observation and modeling in the Tibetan Plateau, *Agr Forest Meteorol*,150(1), 38-46,  
560 <https://doi.org/10.1016/j.agrformet.2009.08.004>, 2010.
- 561 Yao, T. D., Li, Z. G., Yang, W., Guo, X. J., Zhu, L. P., & Kang, S. C., et al.: Glacial distribution and mass balance  
562 in the Yarlung Zangbo river and its influence on lakes, *Chinese Sci Bull*, 55(20), 2072–2078,  
563 <https://doi.org/10.1007/s11434-010-3213-5>, 2010.
- 564 Yao, T. D., Pu, J., Lu, A., Wang, Y., & Yu, W.: Recent glacial retreat and its impact on hydrological processes on  
565 the tibetan Plateau, China, and surrounding regions, *Arct Antarct Alp Res.*, 39(4), 642-650,  
566 [https://doi.org/10.1657/1523-0430\(07-510\)\[YAO\]2.0.CO;2,2007](https://doi.org/10.1657/1523-0430(07-510)[YAO]2.0.CO;2,2007).
- 567 Yao, T. D., Thompson, L., Yang, W., Yu, W., Gao, Y., & Joswiak, D.: Different glacier status with atmospheric  
568 circulations in tibetan plateau and surroundings, *Nat Clim Change*, 2(9), 663–667,  
569 <https://doi.org/10.1038/NCLIMATE1580>, 2012.
- 570 Ye, Q., Zong, J., Tian, L., Cogley, J. G., Song, C., & Guo, W.: Glacier changes on the Tibetan Plateau derived  
571 from Landsat imagery: Mid-1970s - 2000-13, *J Glaciol*, 63(238), 273–287, <https://doi.org/10.1017/jog.2016.137>,



572 2017.

573 Yu, W., Yao, T., Kang, S., Pu, J., Yang, W., & Gao, T., et al.: Different region climate regimes and topography  
 574 affect the changes in area and mass balance of glaciers on the north and south slopes of the same glacierized  
 575 massif (the West Nyainqentanglha Range, Tibetan Plateau), *J Hydrol*, 495, 64-73,  
 576 <https://doi.org/10.1016/j.jhydrol.2013.04.034>, 2013.

577 Zhang, G., Yao, T., Shum, C. K., Yi, S., Yang, K., & Yu, J., et al.: Lake volume and groundwater storage variations  
 578 in tibetan plateau's endorheic basin, *Geophys Res Lett*, 44(11), 5550-5560, 44(11), 5550–5560,  
 579 <https://doi.org/10.1002/2017GL073773>, 2017.

580 Zhang, Q., & Zhang, G.: Glacier elevation changes in the western nyainqentanglha range of the Tibetan Plateau  
 581 as observed by TerraSAR-X/TanDEM-X images, *Remote Sens Lett*, 8(12), 1143-1152.  
 582 <https://doi.org/10.1080/2150704X.2017.1362123>, 2017.

583 Zhang, S.Q., Gao, X., Ye, B.S., Zhang, X.W., Stefan, H.: A modified monthly degree-day model for evaluating  
 584 glacier runoff changes in China part II: application, *Hydrol Process*, 26(11), 1697-1706,  
 585 <https://doi.org/10.1002/hyp.8291>, 2011.

586 Zhao, Q., Ding, Y., Wang, J., Gao, H., Zhang, S., & Zhao, C., et al.: Projecting climate change impacts on  
 587 hydrological processes on the Tibetan Plateau with model calibration against the glacier inventory data and  
 588 observed streamflow, *J Hydrol*, 573, 60-81, <https://doi.org/10.1016/j.jhydrol.2019.03.043>, 2019.

589 Zhou, S., Kang, S., Feng, C., & Joswiak, D. R.: Water balance observations reveal significant subsurface water  
 590 seepage from Lake Nam Co, south-central Tibetan Plateau, *J Hydrol*, 491(1), 89-99,  
 591 <https://doi.org/10.1016/j.jhydrol.2013.03.030>, 2013.

592 Zhou, Y., Hu, J., Li, Z., Li, J., Zhao, R., & Ding, X.: Quantifying glacier mass change and its contribution to lake  
 593 growths in central Kunlun during 2000–2015 from multi-source remote sensing data, *J Hydrol*, 570, 38–50,  
 594 <https://doi.org/10.1016/j.jhydrol.2019.01.007>, 2019.

595 Zhou, Y., Li, Z., Li, J., Zhao, R., & Ding, X. Glacier mass balance in the Qinghai–Tibet Plateau and its  
 596 surroundings from the mid-1970s to 2000 based on Hexagon KH-9 and SRTM DEMs, *Remote Sens Environ*, 210,  
 597 96-112, <https://doi.org/10.1016/j.rse.2018.03.020>, 2018.

598 Table 1 Glacier area changes over the WNT from 1976 to 2020

	1976	2000	2020	1976-2000	2000-2020	1976-2020
	Area(km <sup>2</sup> )	Area (km <sup>2</sup> )	Area (km <sup>2</sup> )	△Area (% a <sup>-1</sup> )	△Area (% a <sup>-1</sup> )	△Area (% a <sup>-1</sup> )
The WNT	884.90±	770.03±33.44	589.17±31.72	-0.54± 0.21	-1.17± 0.30	-0.76± 0.11
Lhasa River	662.23±21.95	580.81±22.79	447.93±21.74	-0.51± 0.20	-1.14± 0.27	-0.74± 11
Nam Co	222.58±7.76	189.22±7.62	141.22±7.10	-0.62± 0.20	-1.27± 0.32	-0.83± 0.11



599 Table 2 Glacier elevation change, mass balance and total mass change over the WNT from 1976 to 2020

	1976-2000			2000-2020		
	Elevation change (m a <sup>-1</sup> )	Mass Balance (m w.e.a <sup>-1</sup> )	Total mass change (Gt a <sup>-1</sup> )	Elevation change (m a <sup>-1</sup> )	Mass Balance (m w.e.a <sup>-1</sup> )	Total mass change (Gt a <sup>-1</sup> )
The WNT	-0.31 ± 0.10	-0.26 ± 0.09	-0.24 ± 0.08	-0.44 ± 0.13	-0.37 ± 0.12	-0.29 ± 0.09
Lhasa River	-0.29 ± 0.12	-0.25 ± 0.10	-0.21 ± 0.10	-0.40 ± 0.16	-0.34 ± 0.14	-0.26 ± 0.09
Nam Co	-0.36 ± 0.17	-0.31 ± 0.15	-0.06 ± 0.02	-0.52 ± 0.18	-0.44 ± 0.16	-0.06 ±

600 Table 3 Statistics of area, quantity, and mass balance of different types of glaciers

Glacier type	1976-2000			2000-2020		
	Area (km <sup>2</sup> )	Number	Mass Balance (m w.e.a <sup>-1</sup> )	Area (km <sup>2</sup> )	Number	Mass Balance (m w.e.a <sup>-1</sup> )
Lake terminating	70.29 ± 2.69	46	-0.36 ± 0.26	49.6 ± 1.82	34	-0.56 ± 0.31
Debris cover	55.42 ± 1.25	5	-0.20 ± 0.34	51.59 ± 1.77	5	-0.44 ± 0.47
Debris cover and lake terminating	5.46 ± 0.32	1	-0.18 ± 0.80	6.05 ± 0.32	1	-0.34 ± 0.92
Regular	615.29 ± 20.73	617	-0.30 ± 0.10	554.64 ± 22.93	692	-0.42 ± 0.12

601

602 **Figure captions**

603 Figure 1 Overview of study area and glacier distribution. Label I in the large, red rectangle represents the SW  
 604 section of the WNT, and Label II in the small, dark red rectangle represents the NE section.

605 Figure 2 Glacier distribution in the WNT in 1976, 2000, 2009, 2014 and 2020. (a) Number and area of glaciers  
 606 by size category. (b) Distribution of glacier area with altitude. (c) Distribution of glacier area with slope. (d)  
 607 Distribution of glacier area with aspect. Data in 2009 came from RGI6.0.

608 Figure 3 The distribution of glacier area change in the WNT from (a) 1976 to 2000, (b) from 2000 to 2020.

609 Figure 4 Glacier area changes with (a) time, (b) elevation, (c) slope and (d) aspect. The short lines on either side  
 610 of the point indicate the margin of error in figure (a, b, c)

611 Figure 5 Mean annual glacier surface elevation changes in the WNT from (a) 1976 to 2000, and (b) 2000 to 2020.  
 612 Label I represents the SW section and label II represents the NE section of the WNT (on the same scale). The red  
 613 rectangular box shows an area of the central WNT referred to in the paper.

614 Figure 6 Glacier elevation change with altitude (m a.s.l) in the whole WNT, inside Nam Co drainage basin and  
 615 outside Nam Co drainage basin from (a) 1976 to 2000 and (b) 2000 to 2020. The dots represent the mean elevation  
 616 change in each 50-m elevation bin and shaded regions in the altitudinal distributions indicate the uncertainty.



617 Figure 7 The distribution of glacier-wide mass balance for individual glaciers ( $> 2 \text{ km}^2$ ) in the WNT from (a)  
618 1976 to 2000, and (b) from 2000 to 2020. Label I represents the SW section and label II represents the NE section  
619 of the WNT (on the same map scale).

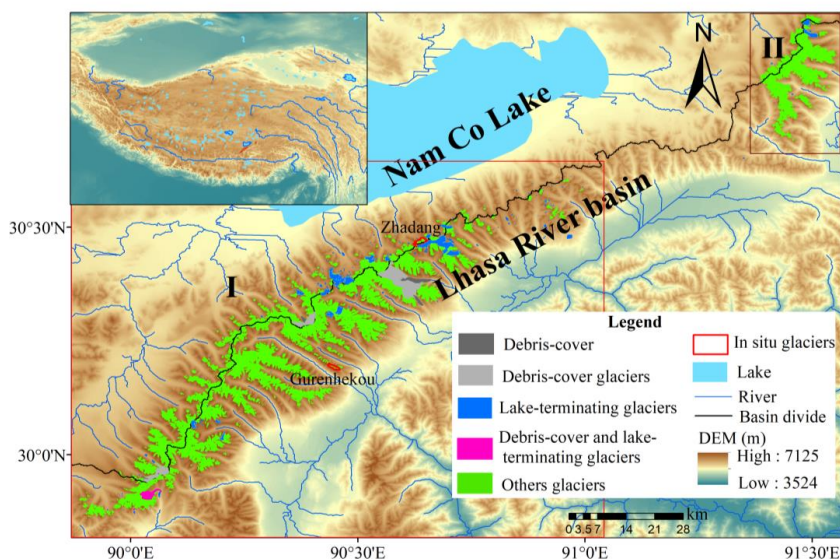
620 Figure 8 Glacier elevation change from 1976 to 2000 and from 2000 to 2020 with (a) elevation, (b) slope, and  
621 (c) aspect. The dots in figure (a) represent the mean elevation change in each 50-m bin and shaded region in (a)  
622 indicate the uncertainty in the altitudinal distributions. (b) is boxplot of  $dh$  in  $2^\circ$  slope bins and four lines from  
623 bottom to top for one box represent minimum value, 25th percentile, 75th percentile, and maximum value,  
624 respectively and dots in figure (c) represent the mean elevation change in each  $2^\circ$  slope bin. (c) represent the  
625 mean elevation change in each  $45^\circ$  aspect bin.

626 Figure 9 Rate of glacier elevation change with elevation of different glaciers types during (a) 1976-2000 and (b)  
627 2000-2020. Plots represent the mediums of glacier elevation change in each 50-m elevation bin and shaded regions  
628 indicate the uncertainty in the altitudinal distributions.

629 Figure 10 (a) Glacier elevation change in the WNT during 2000-2014. (b) Glacier elevation changes with  
630 altitude in the WNT, inside Nam Co drainage basin and outside Nam Co drainage basin from 2000 to 2014. The  
631 dots represent the mean elevation change in each 50-m elevation bin and shaded regions indicate the uncertainty  
632 in the altitudinal distributions. (c) Total area of glaciers and that area covered by the datasets during 1976-2000  
633 and 2000-2014

634 Figure 11 Temperature and precipitation changes for the study area at Damxung, Lhasa and Bange stations from  
635 1976 to 2020. Annual average temperature and precipitation (a, b), ablation season (June to September) average  
636 temperature and precipitation (c, d), accumulation season (January to May and October to December) average  
637 temperature and precipitation (e, f).

638 Figure 12 Gridded temperature and precipitation change during specific time periods.

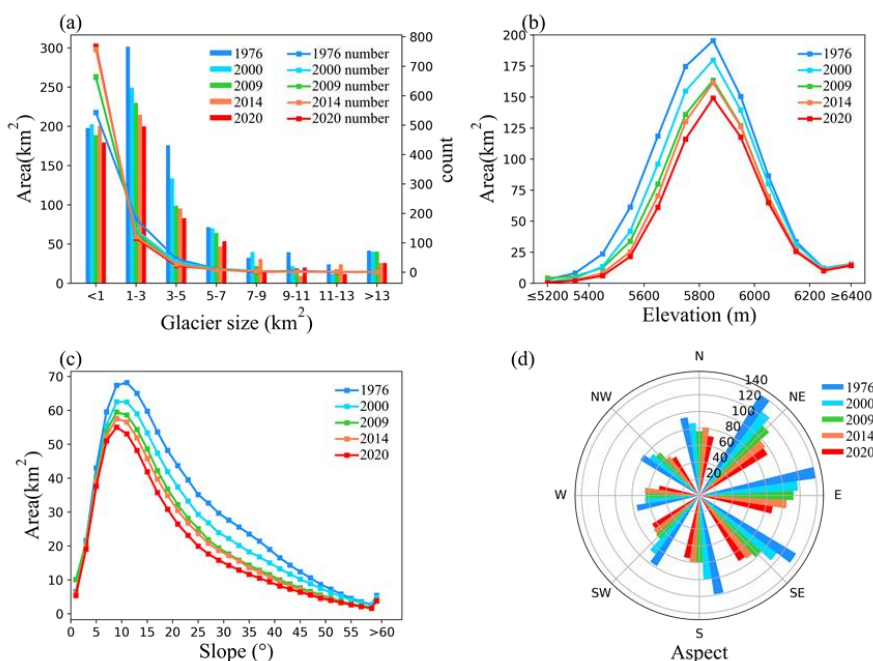


639

640 Figure 1 Overview of study area and glacier distribution. Label I in the large, red rectangle represents the SW

641 section of the WNT and Label II in the small, dark red rectangle represents the NE section.

642



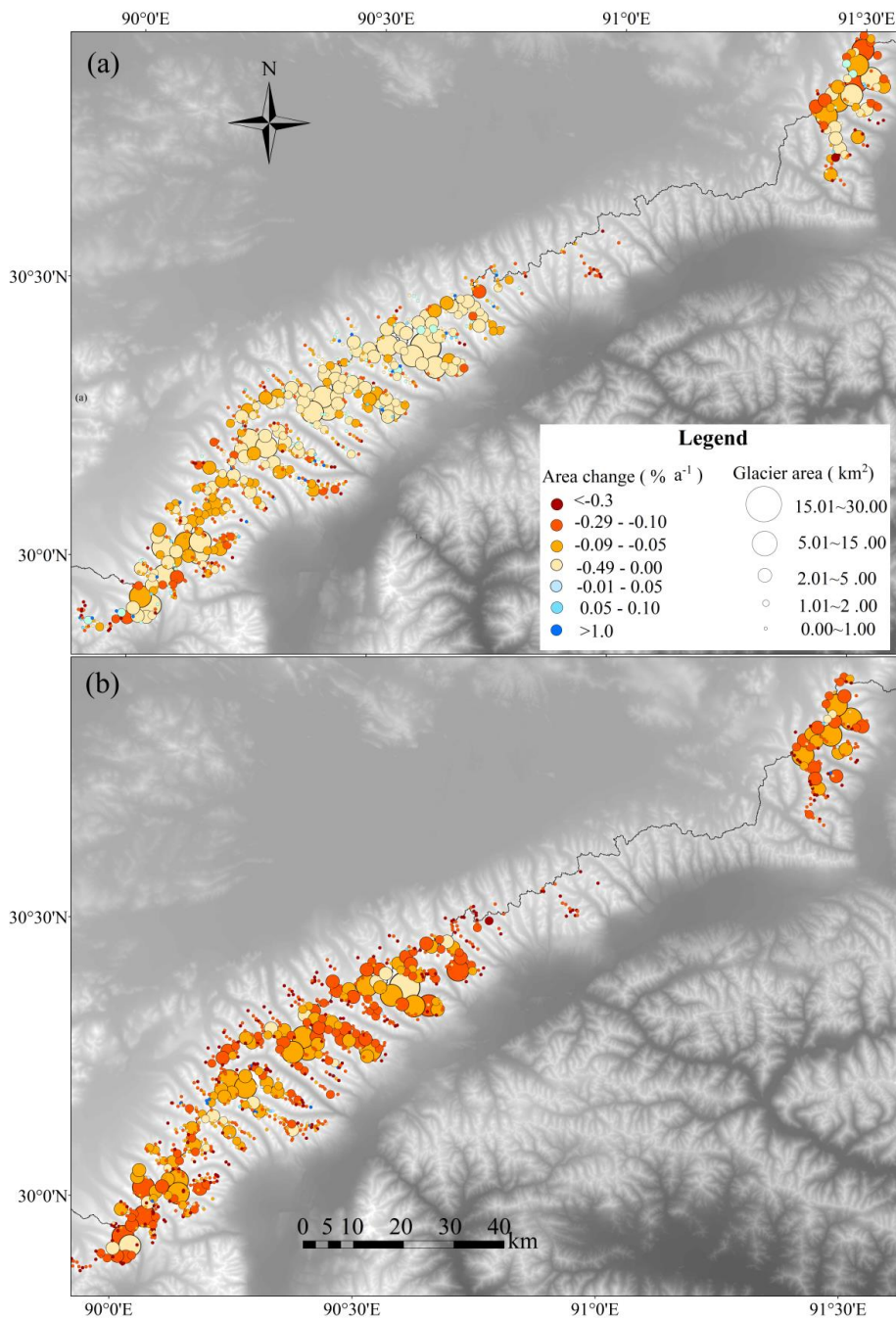
643

644 Figure 2 Glacier distribution in the WNT in 1976, 2000, 2009, 2014 and 2020. (a) Number and area of glaciers

645 by size category. (b) Distribution of glacier area with altitude. (c) Distribution of glacier area with different slope.

646 (d) Distribution of glacier area with aspect. Data in 2009 came from RGI6.0.

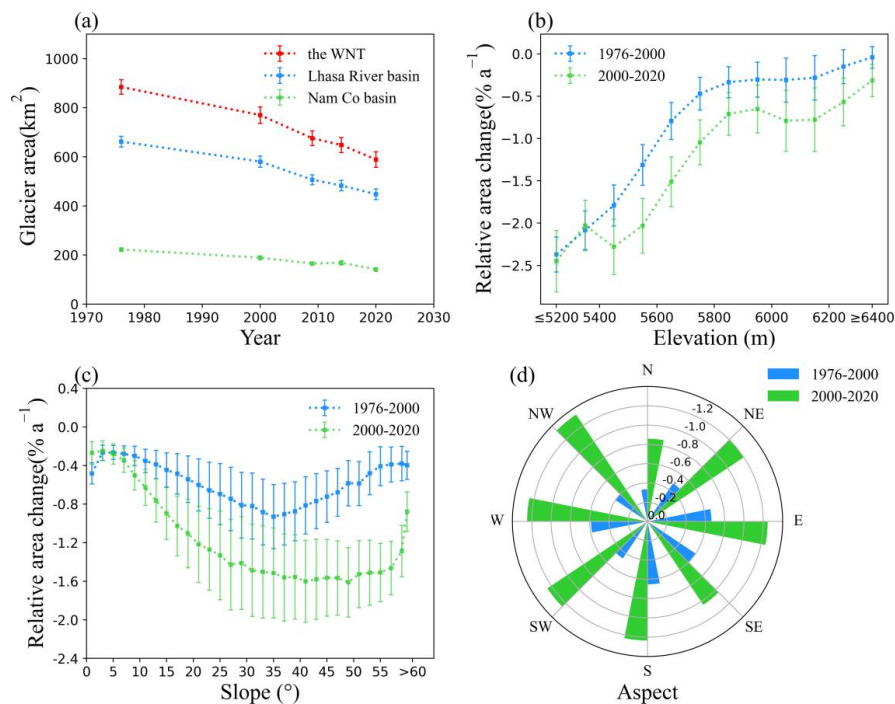




647

648 Figure 3 The distribution of glacier area change in the WNT from (a) 1976 to 2000, and (b) from 2000 to 2020.

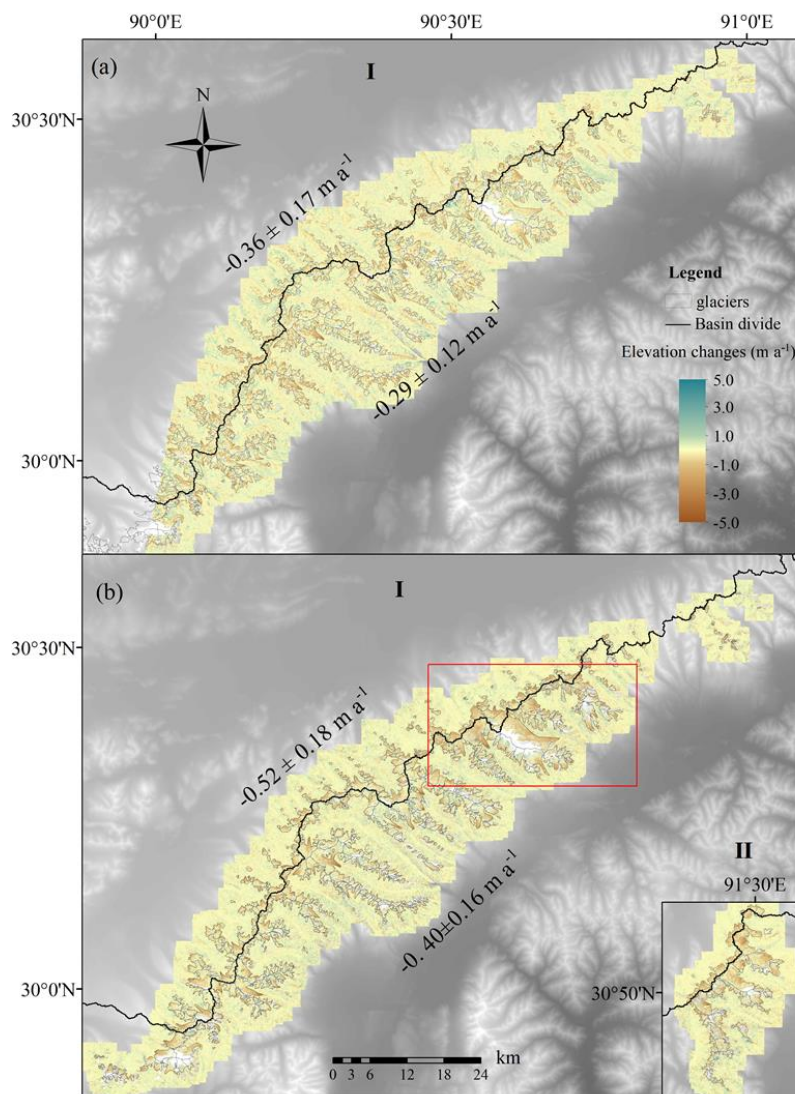




649

650 Figure 4 Glacier area changes with (a) time, (b) elevation, (c) slope and (d) aspect. The short lines on either side

651 of the point indicate the margin of error in figure (a, b, c).

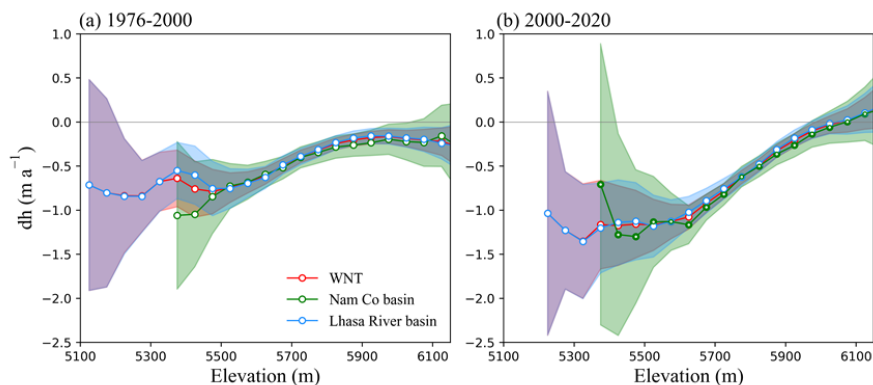


652

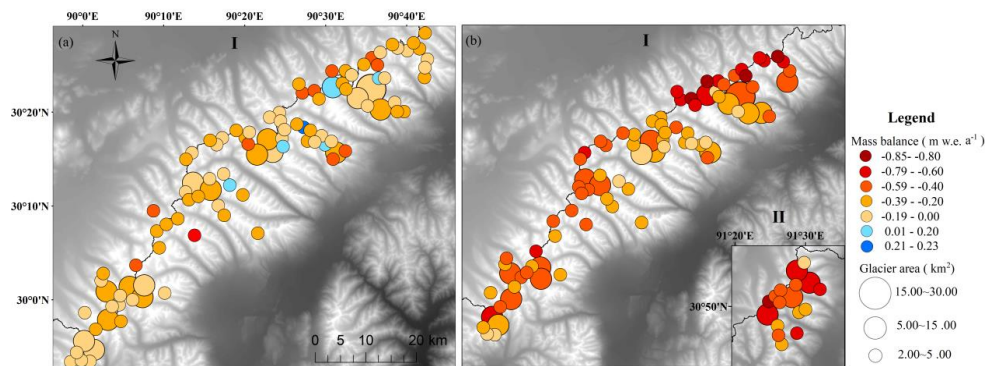
653 Figure 5 Mean annual glacier surface elevation changes in the WNT from (a) 1976 to 2000, and (b) 2000 to

654 2020 (b). Label I represents the SW section and label II represents the NE section of the WNT (on the same scale).

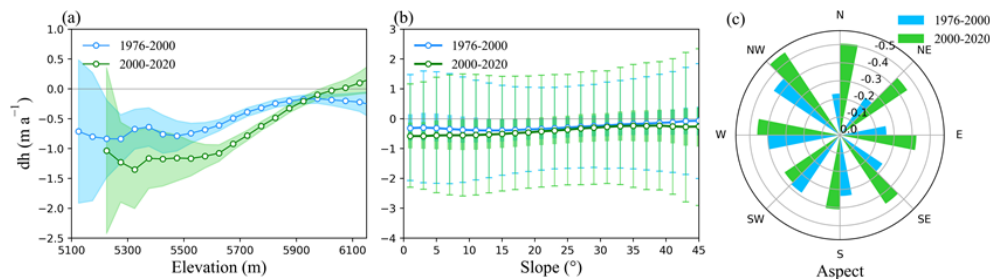
655 The red rectangular box shows an area of the central WNT referred to in the paper.



656  
 657 Figure 6 Glacier elevation changes in relation to elevation (m a.s.l.) in the whole WNT, inside Nam Co drainage  
 658 basin and outside Nam Co drainage basin from (a) 1976 to 2000 and (b) 2000 to 2020 (b). The dots represent the  
 659 mean elevation change in each 50-m elevation bin and shaded regions in the altitudinal distributions indicate the  
 660 uncertainty.



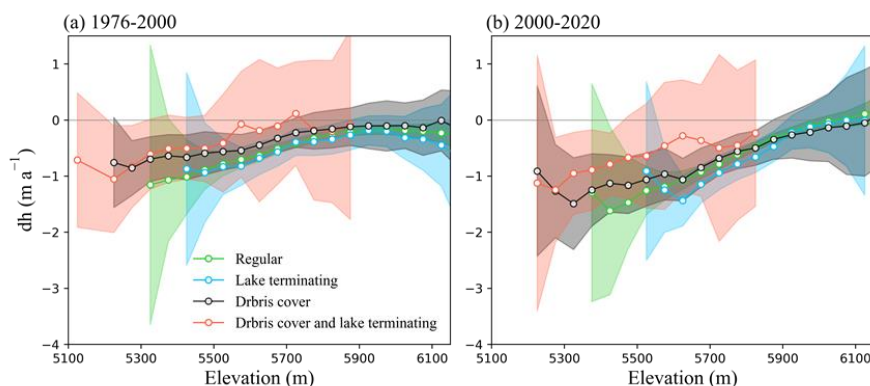
661  
 662 Figure 7 The distribution of glacier-wide mass balance for individual glaciers (> 2 km<sup>2</sup>) in the WNT from (a)  
 663 1976 to 2000 and (b) 2000 to 2020. Label I represents the SW section and label II represents the NE section of the  
 664 WNT (on the same map scale).



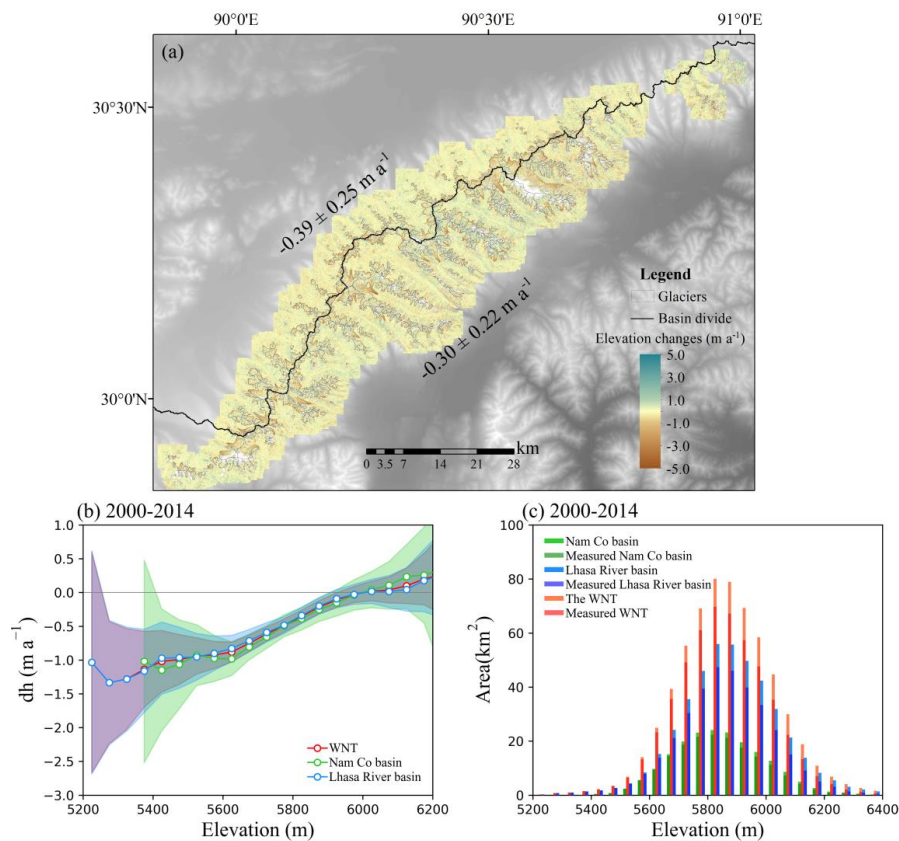
665  
 666 Figure 8 Glacier elevation changes from 1976 to 2000 and from 2000 to 2020 with (a) elevation, (b) slope and  
 667 (c) aspect. The dots in figure (a) represent the mean elevation change in each 50-m bin and shaded region in (a)



668 indicate the uncertainty in the altitudinal distributions. (b) is boxplot of  $dh$  in  $2^\circ$  slope bins and four lines from  
669 bottom to top for one box represent minimum value, 25th percentile, 75th percentile, and maximum value,  
670 respectively and dots in figure (c) represent the mean elevation change in each  $2^\circ$  slope bin. (c) represent the  
671 mean elevation change in each  $45^\circ$  aspect bin.

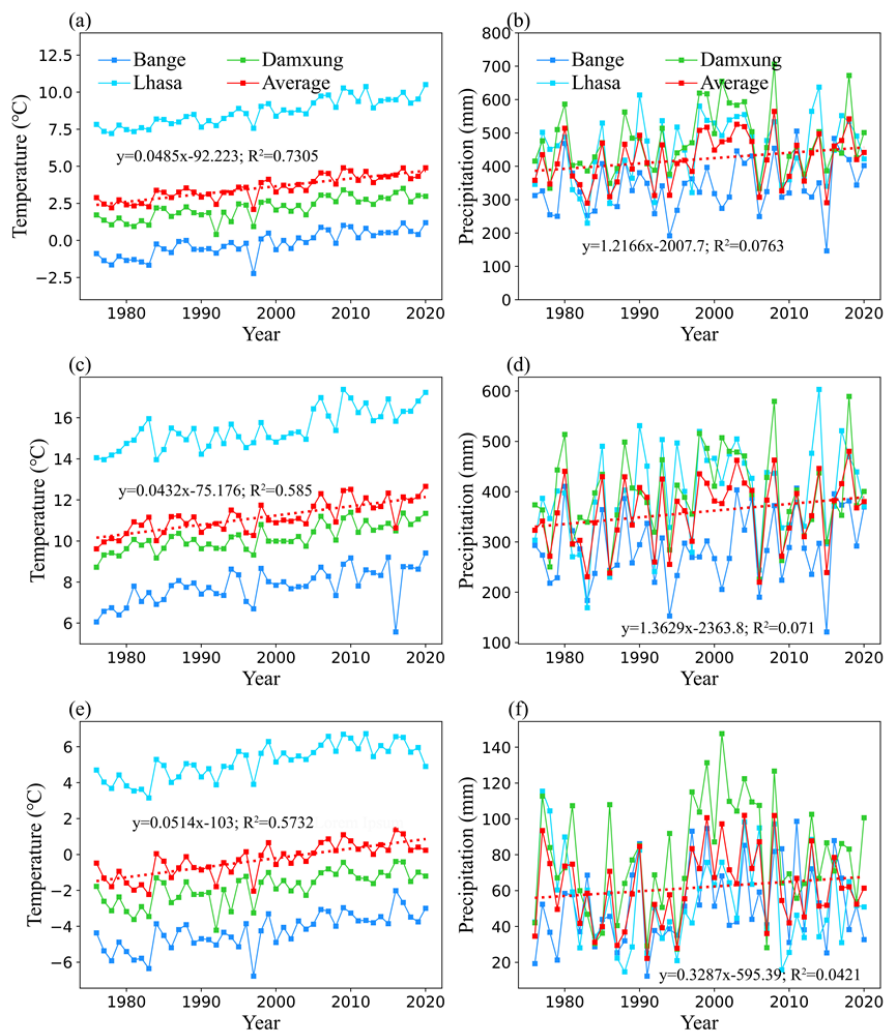


672  
673 Figure 9 Rate of glacier elevation change with elevation of different type glaciers during (a) 1976-2000 and (b)  
674 2000-2020 (b). Plots represent the mediums of glacier elevation change in each 50-m elevation bin and shaded  
675 regions indicate the uncertainty in the altitudinal distributions.



676

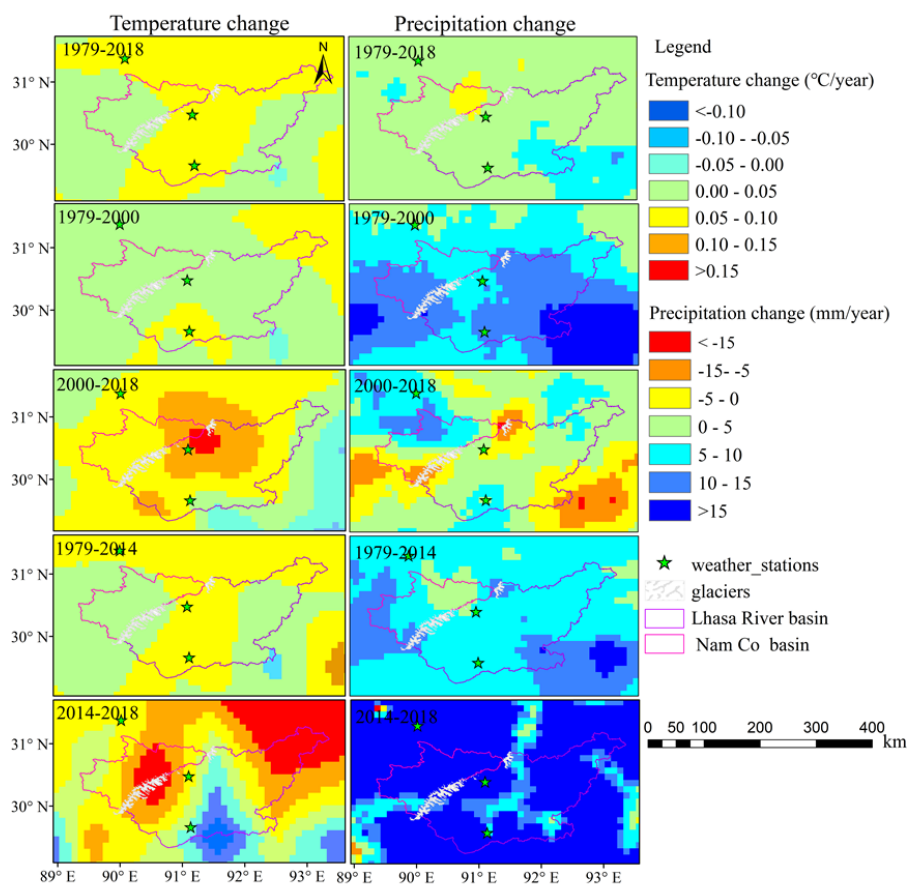
677 Figure 10 (a) Glacier elevation change in the WNT during 2000-2014. (b) Glacier elevation changes in relation  
678 to elevation with altitude in the WNT, inside Nam Co drainage basin and outside Nam Co drainage basin  
679 2000 to 2014. The dots represent the mean elevation change in each 50-m elevation bin and shaded regions  
680 indicate the uncertainty in the altitudinal distributions. (c) Total area of glaciers and that area covered by the  
681 datasets during 1976-2000 and 2000-2014.



682

683 Figure 11 Temperature and precipitation changes for the study area at Damxung, Lhasa and Bange stations  
684 from 1976 to 2020. Annual average temperature and precipitation (a, b), ablation season (June to September)  
685 average temperature and precipitation (c, d), accumulation season (January to May and October to December)  
686 average temperature and precipitation (e, f).





687

688 Figure 12 Gridded temperature and precipitation change during specific time periods.